PRESENTATION OF PROGRESS FOR THE MODELING OF HYPERTROPHIC CARDIOMYOPATHY USING GENOME-EDITED HUMAN INDUCED PLURIPOTENT STEM CELL-DERIVED CARDIOMYOCYTES WITH DYNAMIC MECHANICAL STIMULATION

Nicholas Rogozinski

Thesis Prepared for the Degree of

MASTER OF SCIENCE

UNIVERSITY OF NORTH TEXAS

May 2023

APPROVED:

Huaxiao Yang, Chair
Yong Yang, Committee Member
Amir Jafari, Committee Member
Vijay Vaidyanathan, Chair of the Department of Biomedical Engineering
Shengli Fu, Interim Dean of the College of Engineering
Victor Prybutok, Dean of the Toulouse Graduate School

Rogozinski, Nicholas. *Presentation of Progress for the Modeling of Hypertrophic Cardiomyopathy Using Genome-Edited Human Induced Pluripotent Stem Cell-Derived Cardiomyocytes with Dynamic Mechanical Stimulation*. Master of Science (Biomedical Engineering), May 2023, 41 pp., 1 table, 14 figures, 44 numbered references.

The heart is a dynamic environment that is constantly experiencing some degree of remodeling from the point of development, all the way through adulthood. While many genetic components may contribute to the overall presentation of hypertrophic cardiomyopathy (HCM), mutations occurring in sarcomere components such as myosin binding protein C3 (MYBPC3) are of the greatest popularity for study. Aiming to understand the mechanisms underlying heart diseases and to develop effective treatments that circumvent the need for direct patient study, we investigated the use of a platform to mimic the unique physiological conditions of HCM within an in-vitro setting. Following the induction of mechanical stretch on three human induced pluripotent stem cell derived cardiomyocyte (hiPSC-CM) cell lines containing mutations for MYBPC3 (WT, HET, HOM), all displayed HCM like reactions in calcium waveform. In conclusion, this system demonstrated the potential to apply a constant, static strain to healthy and mutated hiPSC-CMs for the MYBPC3 protein to model HCM in-vitro.

ACKNOWLEDGEMENTS

I would like to acknowledge and thank Dr. Huaxiao “Adam” Yang for his generosity, support, and mentorship throughout my time at the University of North Texas. Thank you for giving me a chance to grow as an individual and contribute to the field of cardiac tissue engineering. Additionally, thank you to all my fellow students who were with me along the way and always reminded me to believe in myself. I would like to thank the members of my thesis committee, Dr. Yong Yang and Dr. Jafari, for both your time and guidance throughout the project.

This thesis is dedicated to my parents and Kevin Hogate.

TABLE OF CONTENTS

Page

LIST OF TABLES AND FIGURES

Page

Tables

Figures

CHAPTER 1

INTRODUCTION

1.1 Real-World Presence of Hypertrophic Cardiomyopathy

The heart is a dynamic environment that is constantly experiencing some degree of remodeling from the point of development, all the way through adulthood. This occurs at many time points such as during development, from constant exercise, or even through pregnancy. Depending on many factors such as genetic profile and diet, this remodeling on both the macro- and micro-scales can become detrimental to the overall function of this vital organ.

Many conditions may affect an individual's cardiac health and well-being, this includes many factors such as genetic inheritance of many significant pathogenic mutations, as well as mechanical stressors on the myocardium. One of the most commonly inherited diseases within this category is hypertrophic cardiomyopathy (HCM)[1]. HCM as a disease is often characterized by abnormal thickening of the myocardial wall and reduced blood ejection efficiency within the left and/or right ventricles. On the cellular level, cardiomyocytes are subjected to mechanical strain typically from pressure or volume overload and are enlarged due to this process[2]. As they are also pulled apart, the interstitial spaces become stiffened due to fibrotic conditions[3].

Estimates near the turn of the century postulated that this disease could be as frequent as 1 out of every 500 people.[4] However, more recent studies have hinted that this value may be grossly underestimating its prevalence among the general population[5] and only further emphasizing the necessity to model the disease in-vitro for better characterization and efficient drug screening practices. In the past, animal models with induced mutations and patient samples have been the primary methods for which we have been able to learn about HCM. While there has been progress, the limitations of these techniques hold us back from the level of

understanding needed to make a significant difference in the lives of patients.

Although the need has been long recognized, only with the advent of human induced pluripotent stem cells (hiPSC) in 2007 have more delicate cell types become readily available for study[6]. Obtaining patient samples has been difficult in the past due to limited availability and inconsistent viability. The advantage of using hiPSCs for disease modeling studies comes with their ability to rapidly proliferate and their pluripotency, or ability to differentiate into many desired cell types. This allows for superior investigation into how genetics play a role in pathologic outcomes, determining the mechanistic pathways, and the potential for personalized treatments. A common shortcoming of many in-vitro models is their inability to gather data and observe cell behaviors in real-time as a condition may arise. Therefore, the usage of a stretcher device that can provide mechanical strain for extended periods can offer insight into how cardiomyocytes (CM) may develop acute and chronic reactions to these stimuli.

1.2 MYBPC3 Mutation and Its Clinical Relevance in HCM

While many genetic components may contribute to the overall presentation of HCM, mutations occurring in sarcomere components such as cardiac β-myosin heavy chain (MYH7) and myosin binding protein C3 (MYBPC3) are of the greatest popularity for study. The prevalence of genetically induced HCM from an MYBPC3 mutation is around 40-50%[7], making it an ideal target of therapy for many researchers investigating ways to combat the disease as it is associated with a myriad of lethal outcomes[8]. To elaborate further, MYBPC3 encodes a regulatory protein that resides within the sarcomere structure, the contractile protein apparatus found within all muscle cells. Within the sarcomere, there are two major components, the thick filaments, and the thin filaments. Thin filaments are comprised of α-actin (ACTC1), the cardiac troponin complex (TNNT2, TNNI3, etc.), and other contractile regulatory proteins. The thick

filaments contain myosin proteins such as MYH7 and notably MYBPC3. In a healthy individual, the thick filaments typically act as anchor points for the thin filaments to slide across, producing the signature contractile motion[9]. MYBPC3 is responsible for maintaining the integrity of the heavy chains and is poised to interact with actin thin filaments to promote and regulate cardiac function. This is accomplished by stabilizing the interaction head motifs of the myosin heads in direct contact with thin actin filaments[10]. Mutations in the MYBPC3 protein most often result in a version with a truncated C'-terminal due to premature termination codon generation. This significantly reduces the quantity of protein binding sites and greatly alters the mechanism of sarcomere relaxation and the alignment of sarcomere filaments[11,12]. HCM induced through MYBPC3 and other frameshift mutations can operate through the genetic mechanism of haploinsufficiency[13], a feature unique to familial inherited HCM. This potentially explains the mutations' overall prevalence among the general population and only further emphasizes the importance of producing an effective model to better characterize this condition.

1.3 Cardiomyocyte Mechanophysiology

CMs reside within a hyperdynamic microenvironment, constantly subjected to constant physical strain and various electrochemical signals. The tumultuous environment is necessary for the growth, development, and maintenance of healthy blood ejection fractions[14]. Therefore, CMs must be more than capable of sensing their environment to reciprocate with the necessary tissue remodeling. While components of this active environment are becoming more established, we still need to develop a further understanding of how mechanoreceptor pathways contribute to the eventual manifestation of a diseased hypertrophic phenotype. While the network of mechanotransduction pathways is extremely complex and a focus of many studies, it remains still critically misunderstood.

We now turn our attention to a component of the mechanotransduction pathway, integrin-dependent focal adhesion kinase (FAK), and its role in cardiomyocyte survival and function. Membrane-bound integrin proteins known as integrins, relay information to the cell in response to changes in the stiffness or microtopography of the extracellular matrix[15]. In turn, FAK promotes increased mitogen-activated protein kinase (MAPK) phosphorylation of multiple pathways to ultimately dictate key functions such as cell survival, contraction-relaxation cycles, and some involvement in the regulation of pro-hypertrophic transcription[16]. The mechanotransduction system is directly connected to structural myofibrils and may offer clues on how mechanical forces alter sarcomere structure and function.

1.4 Disease Modeling for Hypertrophic Cardiomyopathy

Disease modeling of heart tissues has become an increasingly critical area of research, aiming to understand the mechanisms underlying heart diseases and to develop effective treatments that circumvent the need for direct patient study. However, the cardiovascular system is incredibly complex, and the associated pathologies are even more so. Therefore, researchers have focused on generating platforms that aim to analyze a specific aspect of various myopathies. The use of in-vitro-engineered heart tissues allows for a high degree of customization, reduces the ethical burden of using animals for research purposes, and increases the throughput of analysis as direct patient samples are often short in supply.

Existing modeling strategies often incorporate isolated aspects of the disease in question, e.g., biochemical signaling molecules, physical strain, electrical stimulation, etc. To model HCM specifically, many focus on modulating stiffness changes using a variety of substrates and techniques. Our recent study investigated this stiffness change by culturing cardiac fibers on hydrogels of various stiffness[17], as well as utilizing iron particles interlaced in

polydimethylsiloxane (PDMS) to influence substrate stiffness using a magnetic field[18]. In fact, the use of the elastic polymer PDMS has gained significant traction due to its geometric versatility and mechanical compliancy. This compliance is ideal for better characterizing the relationship between mechanical strain and cardiac output. Other researchers have also agreed with this ideology and have utilized stretching to investigate changes in beating dynamics. Martewicz et al. recently utilized the stretching technique to evaluate arrhythmogenesis in response to mechanical stress using transcriptome analysis[19]. They were able to demonstrate the extent to which transcriptional regulation is impacted by mechanotransductive signaling pathways. Additionally, Becker et. al utilized a magnetic-based technique to move PDMS posts fastened to suspended cardiac wires. Their analysis focused on optical observation of contraction through post displacement and emphasized that mechanical strain plays a role in many cellular processes such as CM maturation[20]. These experiments show the potential applications of stretching and constitute a need to better understand mechanotransduction pathways, especially in the context of the pathogenesis of HCM.

CHAPTER 2

FOUNDATION OF STUDY

2.1 Intent of Discovery

This study aimed to mimic the unique physiological conditions of hypertrophic cardiomyopathy within an in-vitro setting. HCM is a condition characterized by abnormal thickening of the ventricular wall[21], partially due to an increase in the size of cardiomyocytes from strain and an increase in tissue stiffness through fibrosis[22]. Both factors play a role in the remodeling of both the myocardial tissue and the sarcomere function. A particular aspect of sarcomere function impacted by HCM is the intracellular calcium dynamics of hiPSC-CMs. An increased sarcomere calcium sensitivity has been associated with MYBPC3-deficient HCM and may indicate a potential aspect of pathogenesis we do not fully yet understand[23]. Therefore, to accurately model the onset of sarcomere dysfunction in the context of HCM, we needed to incorporate a system that could emulate both strain and stiffness change to further characterize how calcium waveforms are manipulated.

2.2 Strategy of Investigation

To investigate calcium dynamics for hiPSC-CMs in response to hypertrophic conditions, the stretcher platform was chosen along with the usage of three isotypes for the MYBPC3 mutation, Wildtype (WT, +/+), Heterozygous (HET, +/-), and Homozygous (HOM, -/-). By utilizing hiPSC-CMs with a known we can examine how mechanical stressors influence calcium cycling within CMs as disruptions in this process can be linked to a variety of heart diseases[24]. The reason calcium handling is of importance is its primary role in the regulation of the contraction-relaxation cycle. Upon external stimuli, calcium is released from the sarcoplasmic reticulum and floods into the sarcomeres. From there, calcium binds to the myofibril protein

troponin C and initiates sarcomere contraction[25]. Our understanding of calcium handling in hiPSC-CMs is underdeveloped and further characterization is needed if we are to take full advantage of hiPSC usage to model HCM. To do this, we utilized cell lines with genetically encoded calcium indicators (GCaMP) via CRISPR-Cas9 knock-in reporter. This opened the door to live-cell imaging of calcium changes over time and provided an advantage over traditional calcium techniques. Often, these rely upon incubating cells in dye solutions that lose potency overtime[26] and are disruptive to other aspects of their electrochemical signaling indicating a degree of cellular toxicity[27]. With these limitations considered, our model demonstrates exciting potential as a simple and accurate way to investigate the effects of mechanical strain on hiPSC-CMs.

2.3 Design Considerations

A fundamental issue with many existing HCM disease models is their high degree of complexity for initiating actuation and inefficient fabrication times. Any researcher looking to investigate diseases such as HCM or others must consider factors such as resources available to them and the throughput potential of their model. Therefore, this project sought to optimize modeling capabilities and versatility while maintaining low startup costs of time and materials.

Stereolithography (SLA) printing, a relatively inexpensive and scalable technique was selected to fabricate a frame (100mm x 85 mm x 12.5 mm) that can fit within the dimensions of standard tissue culture dishes (150mm x 25mm) to allow for storage in traditional incubators. To house hiPSC-CMs for culture, a PDMS reservoir or “membrane” was constructed with outer dimensions of 23.7mm x 25.5 mm x 4.7 mm and an interior well size of 16 mm x 16 mm x 4.5 mm. This roughly replicated the well dimensions of a 24-well plate, a commonly used piece of tissue culturing equipment with generally higher throughput potential, and allowed for similar

working volume use of media (500 µL). Stainless steel rods (76 mm x 3mm) were incorporated into the frame of the PDMS membrane to ensure an even axial distribution of tensile force as this material will have a low degree of bending tolerance within the range of forces applied to the system. Actuation was modulated by a slider (SLA resin) that hooks onto one of the rods, while the other rod was anchored to the frame. This slider is connected to the head of a threaded machine screw (M4 x 50mm) via a ball bearing (4mm interior diameter) to allow for free rotation. The tail end of the screw was attached to the frame using an interiorly threaded rivet nut (M4) and capped with a lock nut (M4). Twisting in the counterclockwise direction would allow for displacement of the slider and generates stretch for the PDMS membrane.

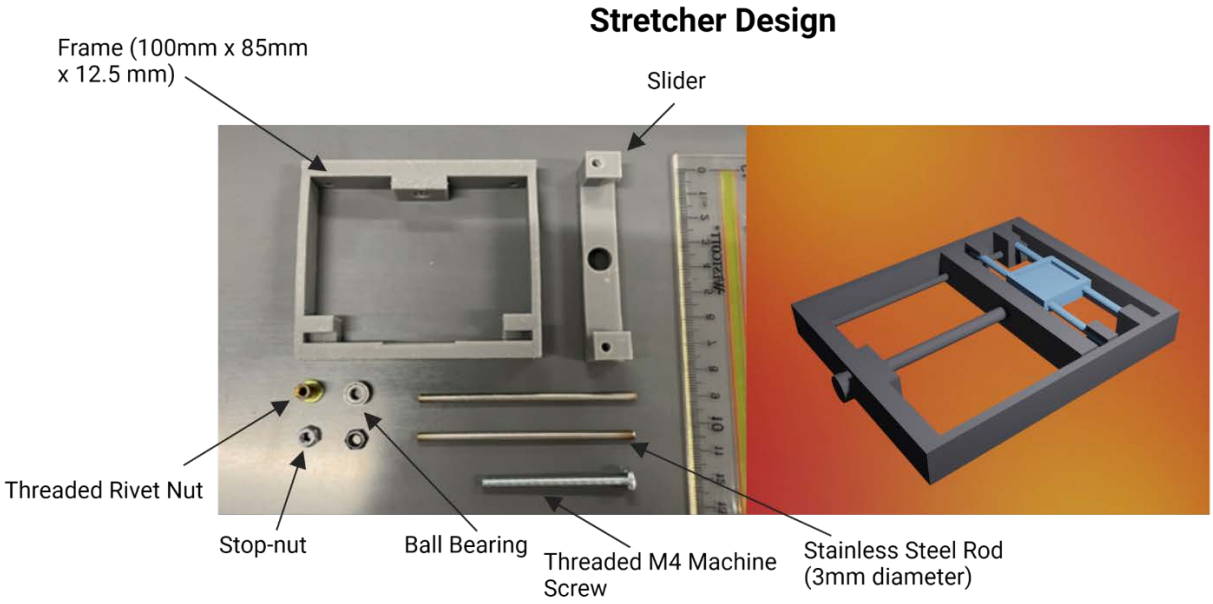

Figure 2.1: Overview of components that comprise the stretcher platform (left) and a computer model of the assembled platform (right). Custom SLA printed components are the "frame" (left image, pictured top-left) and the slider (left image, top-right).

CHAPTER 3

METHODOLOGY

3.1 hiPSC-CM Culture and Differentiation Protocol

For this study, three isogenic human induced pluripotent stem cell lines were obtained from Gladstone Institutes. These included the wildtype (WT, MYBPC3 +/+), heterozygous (HET, MYBPC3 +/-), and homozygous (HOM, MYBPC3 -/-) lines, all of which were produced via CRISPR-Cas9 editing techniques as described in the paper by Ma, Z et al[28].

To promote adherence to the substrate, Matrigel matrix (Corning) was diluted at a ratio of 1:200 with Dulbecco's phosphate-buffered saline (DPBS) (Gibco), and a volume of 1.5 ml was deposited into an individual well of a six-well plate for a 30 min incubation time within the incubator. Prior to seeding, cells were removed from liquid nitrogen storage and the vials thawed as quickly as possible via the use of a 37^{o}C water bath, stirring until the ice was completely dissipated. Cells were then transferred with a micropipette into a 15 ml tube (Falcon) containing room-temperature E8 media with supplement (Gibco) and 10μM dihydrochloride salt Y-27632 (ROCK inhibitor). The mixture was then centrifuged at 280g for 4min. The supernatant was removed via aspiration to carefully leave the remaining cell pellet and was resuspended with E8 + supplement + ROCK inhibitor. Then, the suspended cell mixture was seeded into the well of a 6-well plate following the removal of the Matrigel solution. Media was changed daily using E8 + supplement until cells reached a confluency of roughly 95%. To passage for expansion, the media was removed, and cells were washed with 1 ml DPBS and followed with an incubation of 10 mM EDTA in DPBS for 7 minutes. Next, the EDTA was aspirated, and the cells were gently detached with E8 + supplement + ROCK inhibitor to resuspend the cells for transfer. This was accomplished by placing the media-rich cells into a 15 ml tube (Falcon) containing more E8 +

supplement + ROCK inhibitor media. Once the cells were evenly diluted, the volume was transferred to the 24-well plate in preparation for differentiation.

The 24-well plate containing hiPSCs was allowed to incubate with daily media changes until cells reached around 90% confluency. To initiate the differentiation protocol, hiPSCs had their media removed and replaced with RPMI + B27 -insulin + 8 µM CHIR99021 (GSK-inhibitor/WNT activator), this time point is referred to as “Day 0” and subsequent days mentioned are relative to this time point. Two days after (Day 2), media was removed, and cells were refreshed with RPMI + B27 -insulin. On Day 3, media was again removed and RPMI + B27 -insulin + 10uM IWR (WNT inhibitor) was added to promote mesoderm formation and maintain an ideal WNT gradient for Cardiomyocyte generation. Upon Day 5, existing media is removed, and RPMI + B27 -insulin is added. By Day 7, the addition of insulin to RPMI + B27 (+insulin) aids in the redirection of the differentiation process. RPMI + B27 +insulin is then replenished every two days until cellular contraction or “beating” is visible (typically Day 9 but up to Day 13). Assuming beating is sufficient by Day 9, media is aspirated and replaced with RPMI + B27 +insulin -glucose. The removal of glucose is intended to starve unwanted cell types as fatty acid beta-oxidation can be utilized by cardiomyocytes while byproduct cell types are ultimately filtered out. This media is replenished on Day 11, cell morphology and contraction presence are closely monitored. By Day 13, cells are ready to be transferred to the PDMS substrate or frozen for later use.

3.2 Generation of PDMS and Micropattern Casting

For the basis of applying mechanical stretching to cardiomyocytes, polydimethylsiloxane (PDMS) was selected as the material for use due to its high elasticity and biological inertness. The 184 Silicon Elastomer Kit was purchased from Sylgard and the two components were first

added in a 15 ml Falcon tube at a ratio of 10:1.05 by weight and mixed with a glass stir rod for 5 minutes by hand. Following this, the mixture was centrifuged at 1200 rpm for 4 minutes to remove lingering bubbles.

To generate a micropatterned substrate, a 20 µm by 20 µm feature size was patterned on a silicon wafer with a distance of 100 µm between features using a SU-8 photoresist. This silicon wafer was then placed on a spin-cast device and roughly 2 ml of PDMS was poured onto the center of the wafer. The wafer was spun at 500 rpm for 30 seconds to cover the surface entirely. Next, the covered wafer was removed and placed in a vacuum desiccator to remove bubbles and promote the filling of microfeatures with PDMS. After 1 hour of vacuum time, the wafer was removed and placed on a hotplate at 65^{o}C for 1 hour until PDMS was cured. Using a razor, a square cut was made surrounding the micropatterned region of interest. The excess PDMS was discarded and the square “membrane base” with patterns was carefully removed and placed into 100% Ethanol until use.

3.3 D Modeling and SLA Printing of Stretcher Frame and Membrane Mold

The stretcher frame, stretcher slider, and membrane models were generated using Solidworks (Dassault Systèmes) and printed in separate pieces using Grey V4 photocurable resin (Formlabs) on a Form 3B+ SLA printer (Formlabs). The prints were then sonicated in isopropyl alcohol for 10 minutes and allowed to dry. Finally, prints were placed in a heated UV chamber to finish the curing process for 30 minutes at 60^{o}C.

3.4 Fabrication of Completed Membrane

Stainless steel rods with a diameter of 3mm were purchased from McMaster-Carr and were cut using a rotary tool, then sanded to a length of 76 mm. Two cut rods were placed into the membrane mold, then four silicon “o” rings were placed on the rods at the base of their extrusion

from the mold and sealed with hot glue to prevent leakage of PDMS. Roughly 1.6 ml of PDMS was poured into the mold and then placed into the vacuum desiccator for 1 hour. Once all bubbles were removed, the mold was placed onto a hotplate at 75oC and left overnight. Once cured, the membrane was carefully removed from the mold with the use of a razor and lubricated with 100% Ethanol to improve the consistency and quality of the finished product. The removed membrane frame was trimmed of any excess PDMS and allowed to dry.

The square membrane base was then cut and placed feature-side up within a culture dish. Uncured PDMS was applied to the base of the membrane frame and subsequently placed on the patterned square within the dish, then onto a hot plate at 65^{o}C for roughly 30 minutes. A glass slide with a 50g weight was placed on top to ensure proper bonding of the two pieces during the curing process. After 1 hour of curing time, the membrane was removed from the dish and the PDMS bond was inspected to ensure no leaking of culture media would occur. Excess PDMS was trimmed from the base of the membrane and was placed in 100% Ethanol for storage.

3.5 Cell Culture Preparation and Stretcher Seeding

One well of a 6-well plate was coated with 1.5 ml of 1:100 Matrigel in DPBS and allowed to incubate for 1 hour in an incubator. Cells were sourced from liquid nitrogen storage and were thawed quickly at 37^{o}C. Once completely thawed, the Matrigel solution was replaced with freezing media containing the desired isotype of cardiomyocytes in the 6-well plate. The cells were allowed to rest for 2 days until a visible beating occurred.

The stretcher frames are first disinfected with 70% ethanol and CaviCide spray. The spray is allowed to rest for 5 minutes before removing excess with a Kimwipe and placing the frames into a culture dish (150 x 25mm) within the biohood for later use.

PDMS membranes were cleaned through sonication intervals of 15 minutes each.

Membranes were placed into a container and the process started with the usage of detergents dissolved in RO water. Following this, a ratio of 1:1 then 1:4 (RO water to ethanol) was used to clear the existing debris from the substrate and provide a degree of decontamination. The existing liquid was removed from the sonication container and membranes were allowed to dry before autoclaving occurred. The autoclaved membranes were then placed in a cell culture dish (100 x 20 mm) and were plasma treated for 30 seconds to reduce the water contact angle of the PDMS (typically around 90o to 120o) and improve hydrophilicity. Immediately following this, Matrigel diluted in DPBS at a 1:100 ratio was added to the reservoir within the PDMS membrane and fitted into the stretcher frame. The stretchers were then placed in an incubator overnight or for a minimum of one hour and thirty minutes.

Prior to seeding, the CMs were removed from the incubator, washed with 1 ml of DPBS, and treated with 1 ml TrypLE Select 10x (Gibco) for 8 min in the incubator. The detached cells were transferred in solution to a 15ml Falcon tube and centrifuged at 280 x g for 4 minutes. The supernatant was removed, and the pellet was resuspended using RPMI + B27 +insulin +2% FBS +1% penicillin/streptomycin. Cells were counted using trypan blue and diluted to the appropriate density before transferring 500 µL of cell-containing media to the PDMS membrane and incubator storage. Cells were seeded at a density of 300-400k cells/ml for each run of the experiment.

3.6 Calcium Transient and Morphology Observation

Cells were maintained on stretchers for a period of 13 days in total and analyzed using a Keyence BZ-X800 fluorescence microscope. Images and videos were collected on specific time points as depicted in Figure 2.1 using consistent binning and gain settings at 75 frames per second (fps). Calcium transient videos were recorded at a magnification of 10x for 10 seconds

with a GFP filter. Additionally, phase contrast images were obtained using 10X magnification alongside calcium video collection.

3.7 Analysis of Calcium Transient

Videos collected were initially loaded into ImageJ where individual cells were selected as regions of interest (ROIs) and saved as independent files. A custom MATLAB script created in Dr. Nathan Huebst's lab (Oguntuyo, Schuftan, et al. In Preparation) converted the video, then utilized median filtering and background subtraction to extract waveform characteristics from the ROI videos for calcium waveform amplitude (AMP), decay 50%, uptick duration (UPD), the area under the curve (AUC), and peak time above 80% of amplitude (PT80). Processed data was compiled and normalized to the average value 1 Day before stretching had occurred. The Normalized averages were obtained and graphed using Prism 9 (GraphPad). Calcium transient comparisons between days were made from the same locations on the membrane and between cells exposed to static stretching and cells that were cultured undisturbed. A Student's t-test was used for finding statistical significance between groups. P-values are reported as $p < 0.05$ (*) and $p > 0.05$ (ns). Overview illustrations were made using BioRender (biorender.com).

3.8 Immunostaining

Following completion of video data collection, membranes were washed with 500 µl of DPBS and fixed with the same volume of 4% Paraformaldehyde (Thermo Scientific) solution for a duration of 15 minutes. The membranes were again washed an additional three times for two minutes each, then removed from the stretcher frame and placed in a dish.

Cells were saturated with 500 µl of 0.5% Tritonx-100 in DPBS for a duration of 15 minutes to permeate the cellular membrane and were again washed three times with DPBS. To block non-specific binding, a solution of 1% BSA in DPBS was dispensed onto the stretchers

and allowed to incubate at room temperature for 25 minutes. Following another three rounds of washing with PBS, cells were subjected to 500 µl of phalloidin and anti-human cardiac Troponin T (cTNT) primary antibody (DSHB), then placed in 4^{o}C to bind overnight. The following day, cells were washed three times with DPBS, and 500 µl of Alexa Fluor 667 anti-mouse (ThermoFisher Scientific) antibody solution was added to the cells and allowed to incubate at room temperature for 2 hours. The membranes were then sliced into 4 equal parts and the walls were removed. A glass cover slide was obtained and ProLong™ Gold Antifade Mountant with DAPI (Invitrogen) was placed on the cover slide. Using sterilized tweezers, the segmented membranes were placed on the anti-fade gold solution and allowed to incubate at room temperature for two days. Stained cells were analyzed using a Keyence BZ-X800 fluorescence microscope with blue, green, and red fluorescent filters. Raw images were then passed through a program created by our lab that uses a machine learning algorithm to quantify intensity per area unit.

3.9 Mathematical Modeling

Initially, the displacement of the stretchers was calculated using a video microscope positioned above the system. The membranes were inserted into the stretcher and the apparatus was fixed to the benchtop alongside a ruler. The initial position and position before and after stretching of the slider were recorded via video and measurements of displacement were conducted in ImageJ. Simulations were generated using a negative model of the membrane mold in Solidworks using the built-in simulation feature to observe the membranes' reaction, including stress and strain, to a prescribed displacement.

CHAPTER 4

RESULTS

Figure 4.1 shows an overview of the experimental setup. First, hiPSCs are differentiated using the above-mentioned protocol into cardiomyocytes. From there they are then seeded onto the PDMS membrane that is secured within a frame. The rods spanning the width of the membrane are anchored to both the frame and a slider which can have its displacement tuned by turning a threaded shaft. This allows for the slider to move while stretching the membrane to the desired length. Cells are then imaged using a fluorescent microscope to observe calcium transient changes in response to stretching. Videos are analyzed using a MATLAB script and cells are fixated for immunostaining following 7 days of static prolonged stretching. Made using BioRender (biorender.com).

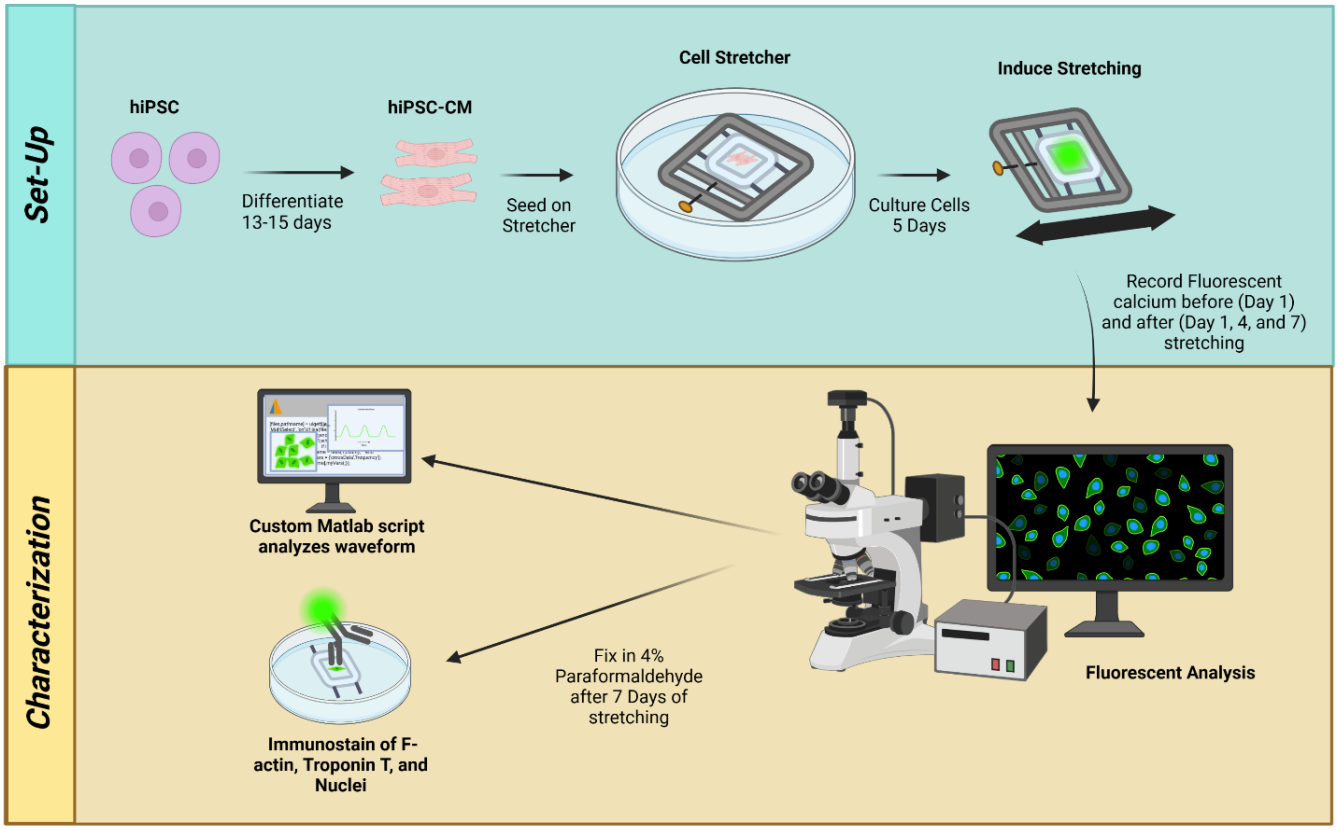

Figure 4.1: Overview of the experimental setup.

4.1 Displacement Capabilities of the Stretcher

Following the fabrication of frames and membranes, stretchers were evaluated on their abilities to perform and maintain the desired stretch. Membranes were placed into the frames and fastened to a benchtop alongside a ruler with metric graduations. A video microscope was used to capture the stretcher in its “pre-stretch” state, meaning the membrane was extended to a point where the PDMS became taut and before visible stretching had occurred. Notch marks were placed on all frames at this point for consistency of the initial membrane position.

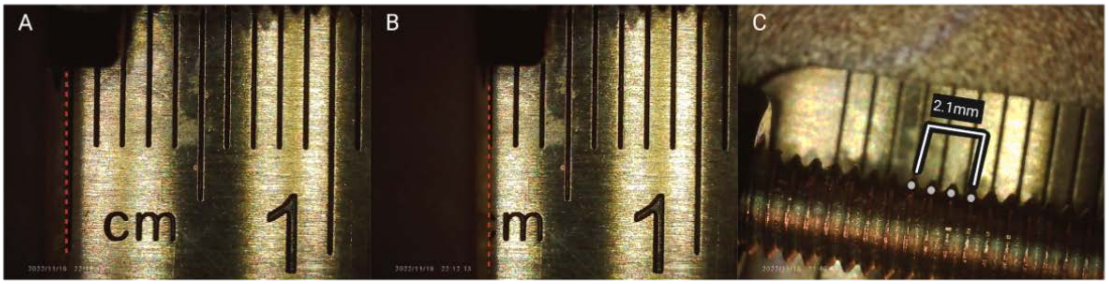

Figure 4.2: Photos of the whole stretcher to show displacement of PDMS membrane before (A) and after (B) stretch. Images were taken from a video microscope at a zoom of 50x digital to show the displacement of the slider. The initial position of the slider is marked with a dotted red line and was displaced 2.1 mm with 3 turns of the threaded shaft to its final position, also marked by a red dotted line. To validate displacement, thread pitch was calculated using ImageJ and compared to the literature standard of an M4 machine screw (C). Made using BioRender (biorender.com).

The stretcher slider was turned 3 times and was analyzed via ImageJ to reveal a displacement of 2.1mm and an overall stretching of 12%. Although the slider was initially measured, the membrane itself was observed to determine if displacement was fully translated. In a comparable manner of analysis, the membrane was revealed to displace 1.9 mm with a stretch of 7.5%. This means a 9.5% loss of loading had occurred, likely due to the hooked area of the slider giving way to the metal rod during strain. To confirm strain was translated through the PDMS, 4 locations were imaged on a dry membrane before and after stretching. All regions were observed to have strain percentages ranging from 7.6% - 7.9%, confirming the mechanical stretch was being transferred.

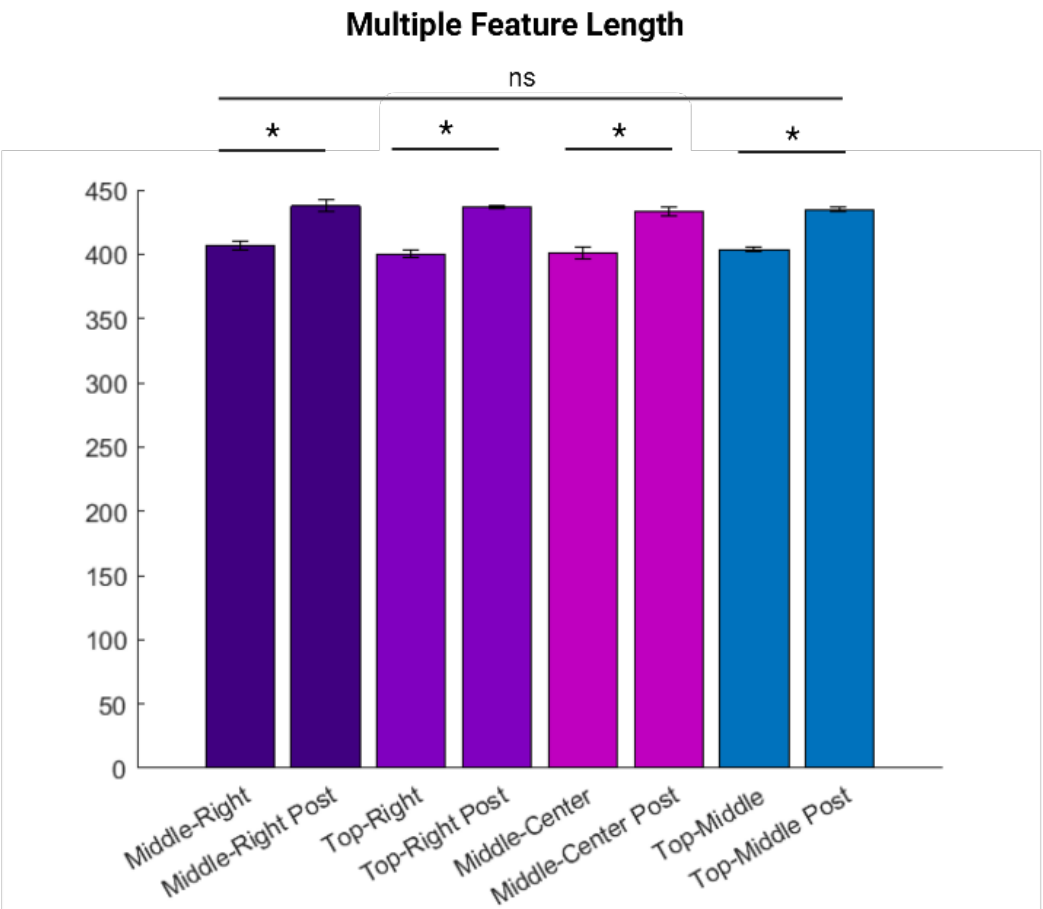

Figure 4.3: Lengths of three repeating features (micropatterned grooves) were recorded in various areas in the PDMS membrane before and after stretching using ImageJ.

4.2 Seeding of Cells onto Stretcher

The use of PDMS offers many advantages as a substrate, however, its hydrophobicity is its greatest concern. Following 5 days after seeding hiPSC-CMs on the membrane, cells were imaged at 10x using the Keyence microscope to observe the quality of cell attachment and morphology after passage to the membrane for 8 randomly selected locations. Cells of all three isotypes (WT, HET, HOM) were able to exist as both clusters, typically displaying a phenotype with relative elongation and synchronized beating, as well as individuals with a more radially elongated morphology (Fig. 4.4). Both types were only slightly different in the previously mentioned aspects and indicated sufficient attachment.

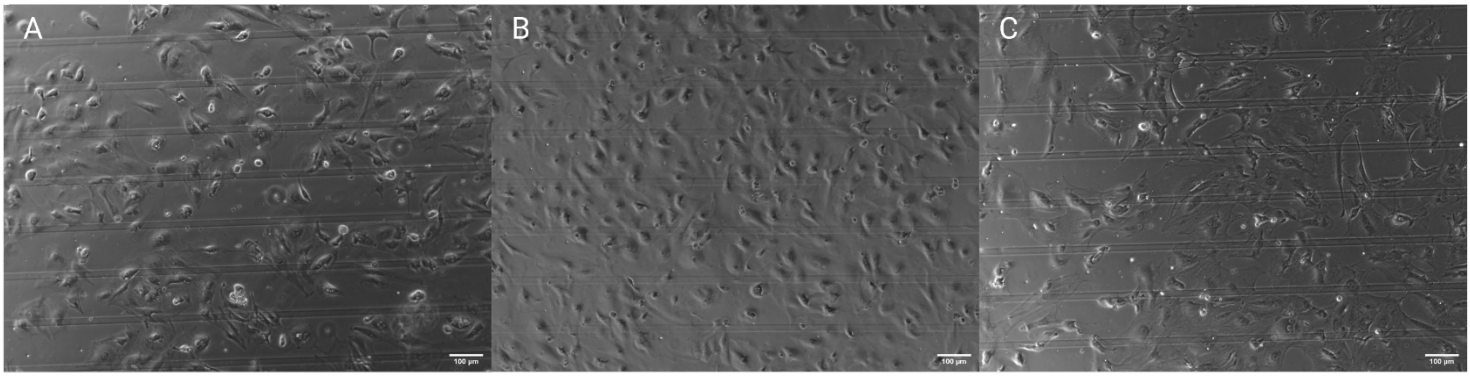

Figure 4.4: Brightfield images (10x) of all three isotypes were taken to demonstrate the initial morphology and validity of the platform as a cellular substrate. Wild Type (A), Heterozygous (B), Homozygous (C). Scale bar represents 100µm. Made using BioRender (biorender.com).

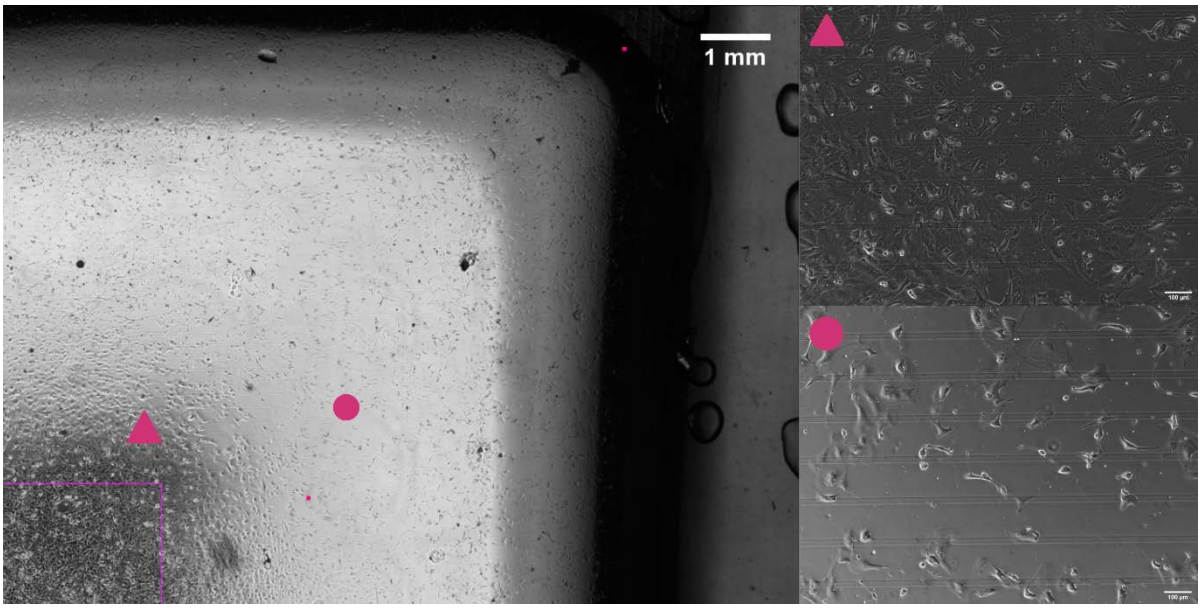

Figure 4.5: Quarter-view image of the membrane produced by stitching together images at 10x magnification. An image taken at 10x magnification in a central area (top right) and a radial part (bottom right) of the membrane is displayed to display the difference between cell densities by region. Scale bars of the displayed regions read 100µm in length. Made using BioRender (biorender.com).

CMs tended to congregate towards the center of the membrane, resulting in a higher cell density and a monolayer-like appearance. Meanwhile, areas that were more radially located tended to have a lower cell density and were intermittently clustered (Fig. 4.5). Additionally, CMs appeared to have a healthy appearance but did not seem to be guided by the micropattern. Some areas of the membrane demonstrated a general alignment of cells while others had cells

that completely ignored the presence of micropatterns, spanning perpendicular to the direction of the patterning. This suggests that the patterning depth of 20µm was insufficient to generate the desired alignment of CM and can be attributed to either the degradation of the master mold or may demonstrate the need to incorporate increased feature depths. Additionally, hiPSC-CMs seeded on stretchers demonstrated a low viability rate (>40%) within the first few days of seeding. Cells may have attached but do not visibly contract or fluoresce from calcium handling. The viability of the experiment seemed able to be determined based on the response of cardiomyocytes in as little as two days after seeding.

4.3 Calcium Transient Analysis

Following initial characterization, CMs were recorded using a green fluorescence filter to observe calcium handling waveform amplitude (AMP), duration of uptick (UPD), time to 50% of decay of the waveform (TD50), the time within 80% of peak (PT80), and total area under each wave (AUC). Components of waveform were extracted using ImageJ to select single CMs and regions of interest were then processed through a pair of custom MATLAB scripts by Huebst et al. The averages of each data point over 8 total days following extraction from the raw videos, were compiled. The first day of data analysis encompasses the status of the cells before stretching was applied to observe as a reference. Following imaging, cells were subjected to mechanical strain by 3 rotations of the centralized threaded shaft and allowed to incubate overnight. The following day, cells were imaged in the same manner to observe acute reactions to increased static strain and substrate stiffness. Cells were again imaged at 4 days and 7 days following the applied stretch to better understand the cellular response in a more long-term setting of these applied variables.

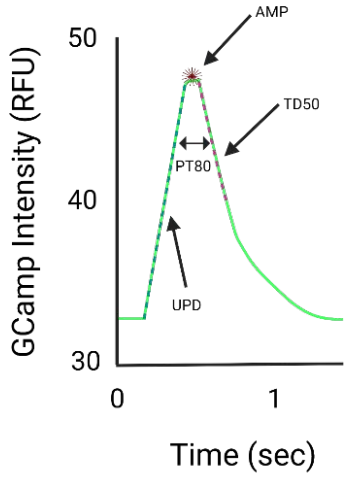

Figure 4.6: Depicted here is the general shape of a waveform obtained from the calcium handling process. Highlighted are various aspects of the wave that are of interest for this study and how they correspond relative to their location on the wave. Image made using BioRender (biorender.com).

4.3.1 Analysis of the Wildtype Cell Line

The use of the WT cell line represents a healthy patient without the presence of a frameshift mutation that would normally truncate the MYBPC3 protein. Initially, cells were evaluated for a duration of 4 days to evaluate their acute response to mechanical strain. Upon the induction of physical stretching, peak amplitude had a significant ($p <= 0.05$) decrease relative to pre-stretch conditions. Day 4 after stretching was the only instance where a significant difference from the non-stretch control was observed. However, this reduction in amplitude may be partially due to the tendency of the membranes to have insufficient media volume due to evaporation. Decay 50 times were relatively maintained following the induction of stretch, this was true for both the stretch and control group. However, at the time point of Day 4 following stretch, a sharp drop-off in decay times was observed. Uptick duration, or the time it takes to go from the start of a wave to its peak amplitude, saw a decrease in time by Day 4 and indicating a faster systolic function. The total area under the curve among the stretched group had no significant changes throughout the course of the experiment. Among the non-stretched group, the

total calcium handled saw a slight decrease but again recovered by Day 4 post. TP80 saw no significant changes among both groups following Day 1 after the stretch. Interestingly, this changed by Day 4 after the stretch where there was a significant reduction.

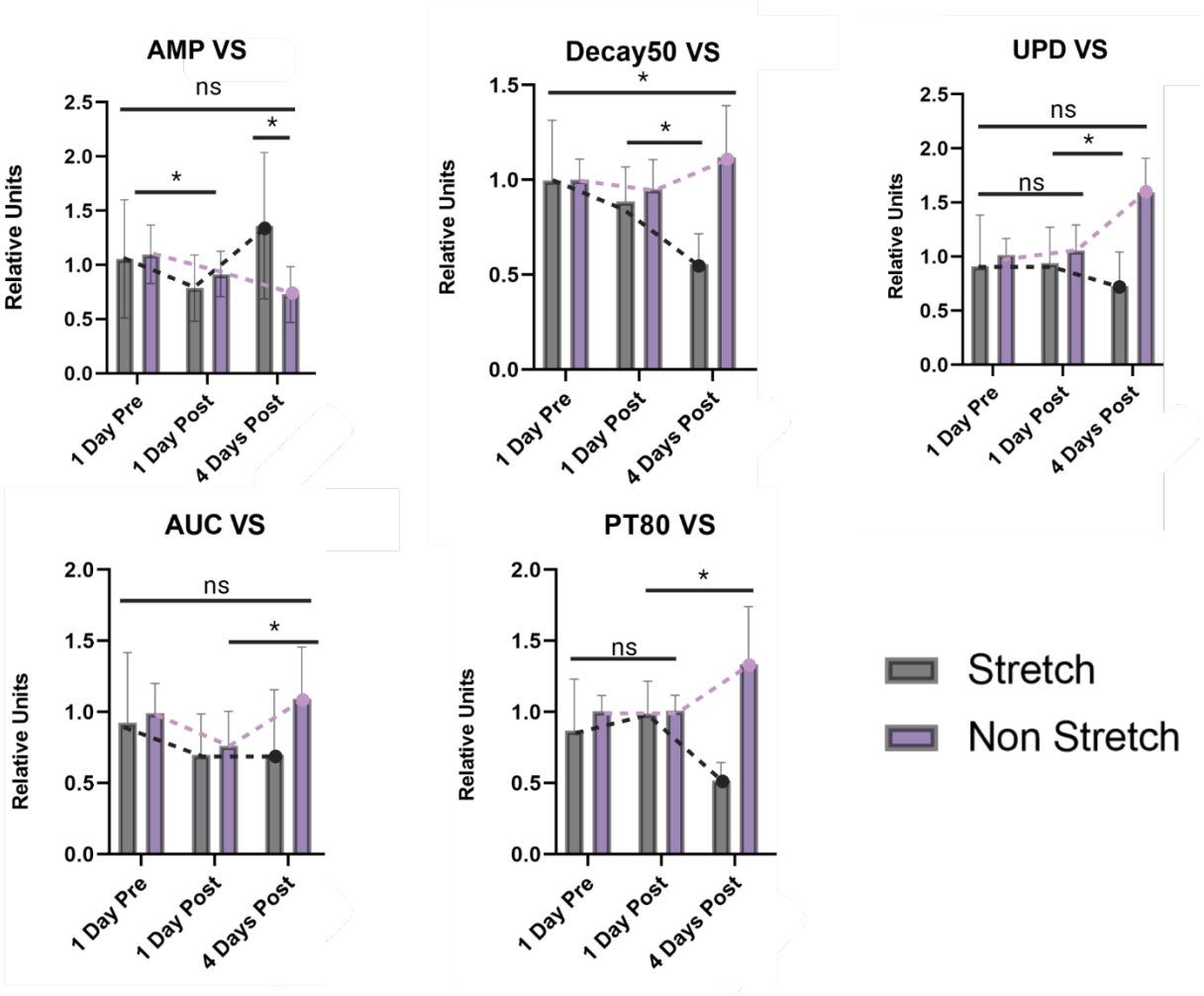

Figure 4.7: Compiled normalized results of waveform components in response to prolonged stretching between the stretched and non-stretched WT isotype. A Student's t-test was used for finding statistical significance between groups. N = 20. P-values are reported as $p < 0.05$ (*) and $p > 0.05$ (ns). Graphs were made using BioRender (biorender.com).

Upon initial observation, there appeared to be a distinction between immediate and prolonged reactions to stretching. We then decided to continue the culturing to Day 7 post stretching to better characterize the trends of chronic strain response. After stretching for an

additional three days, amplitude appeared to recover and conclude at a value seen before stretching. This was indicated by a lack of statistical significance between Day 1 before stretch and Day 7 post stretch. Decay 50 continued its trend through Day 12 without showing signs of recovery. Uptick duration, however, recovered to near pre-stretch times by Day 7 post-stretch. The TP80 decrease indicated a sharpening of the peaks, which was consistent through Day 7 post. Unfortunately, data was unable to be obtained for the non-stretched group following Day 4 post-stretching. This was the result of the membranes drying out, or cells being lost due to unforeseen circumstances. While efforts were made to decrease the probability of membranes drying out, such as with the introduction of DPBS reservoirs on the edge of the culture dishes, cells suffered damage from media loss and became unusable afterward. This significant drawback also helps to explain the relatively large error bars and lack of viable replicates for this section and some others throughout the course of the study. Going forward, other isotypes were evaluated up to Day 7 for a consistent analysis window.

4.3.2 Analysis of the Heterozygous Cell Line

Cells with a heterozygous mutation were analyzed in a similar manner to the WT, stretch was induced and maintained for the duration of 7 days and recorded. Following induction of stretch, the maximum amplitude of the waveforms was observed to have no significant change even by end of the experiment. Decay 50 had a similar response to PT80, seeming to change in the opposite direction of each other. Initially, stretching resulted in a reduction of this decay and PT80 which continued in trend until Day 4 post-stretching. By Day 7 after stretching, there was a slight recovery in both times that resulted in a net lower value throughout the experiment. Uptick duration did not see a meaningful change in the stretched group until Day 4 after the stretch where the value decreased and remained for the remainder of the experiment. As opposed to the

non-stretched group, which saw the UPD slightly increase over time. AUC experienced a decrease and then gradual recovery after stretching, while without the induction of mechanical stress, the area saw a gradual increase.

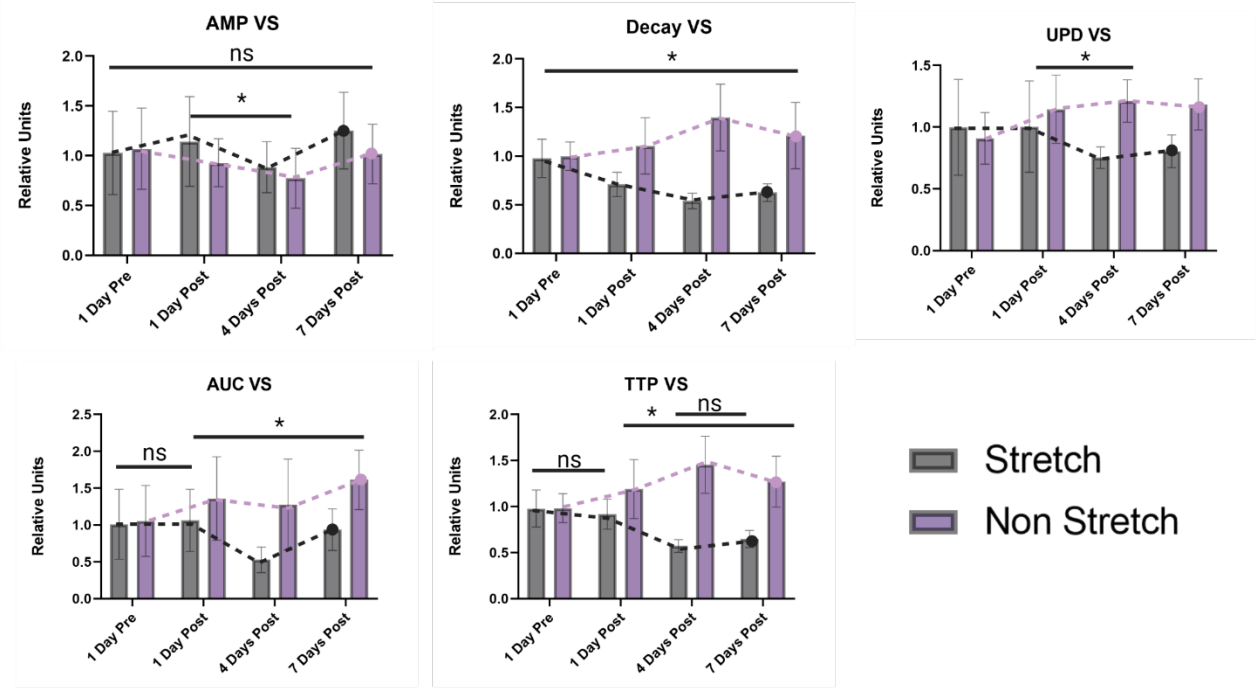

Figure 4.8: Compiled normalized results of waveform components in response to prolonged stretching between the stretched and non-stretched HET isotype. A Student's t-test was used for finding statistical significance between groups. N =20. P-values are reported as p < 0.05 (*) and p > 0.05 (ns). Graphs were made using BioRender (biorender.com).

4.3.3 Analysis of the Homozygous Cell Line

The last of the isotypes analyzed was the homozygous cell line, carrying two dysfunctional alleles for the MYBPC3. First of interest was the unique response of amplitude that occurred in both groups. A significant decrease in amplitude occurred following the onset of stretching and only minor recovery was seen in the non-stretched group. Decay times were relatively stagnant resulting in no significant changes, while the non-stretched group saw an overall reduction by Day 7 of post-stretch culture. This result differs from the change in uptick duration that occurred, concluding the experiment with an overall increase in this metric.

Additionally, it appears that the non-stretch group increased to an even greater extent. As for the total area under the curve there also appeared to be no significant change before and after stretching, nor was there 7 Days post stretching. This was unlike the non-stretch group which experienced a significant reduction in total calcium flux at the Day 1 post-stretch mark and saw significant recovery by Day 7. Importantly, there was a net decrease at the end of the experiment even with recovery present. Lastly, the only meaningful change in PT80 was by Day 4 post stretch in the non-stretched control group.

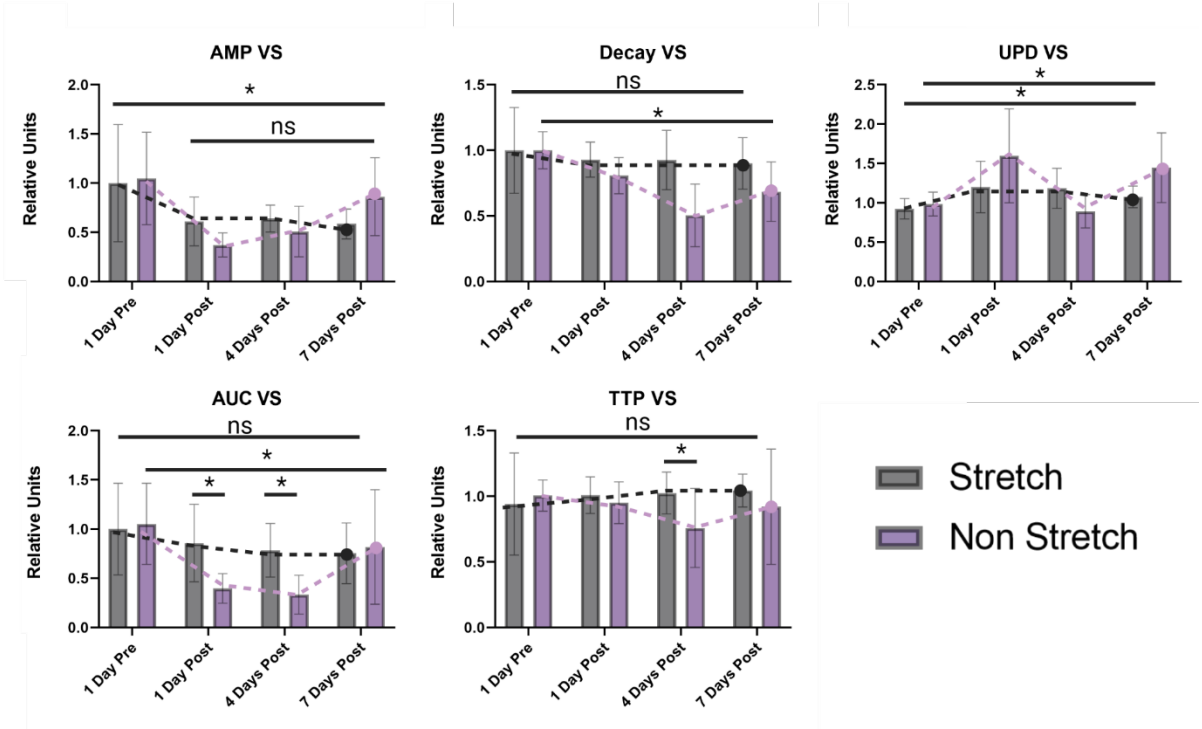

Figure 4.9: Compiled normalized results of waveform components in response to prolonged stretching between the stretched and non-stretched HOM isotype. A Student's t-test was used for finding statistical significance between groups. P-values are reported as $p < 0.05$ (*) and $p > 0.05$ (ns). Graphs were made using BioRender (biorender.com).

4.3.4 Compiled Analysis

To further evaluate the stretcher platform on its ability to exacerbate hypertrophic conditions we looked to compare the various differences in response to stretching among the

three isotypes. Analysis of the non-stretched groups first allows us to establish inherent differences among the cell lines as a direct result of the in-place mutation. This allows for additional information to be inferred about the results of stretching and how the isotype reacts. For both groups, comparisons between each isotype were not made as values were normalized to this time point to allow for relative changes to be observed. Additionally, Day 7 post stretch for WT was not evaluated as there were no replicates capable of producing data up to this time point.

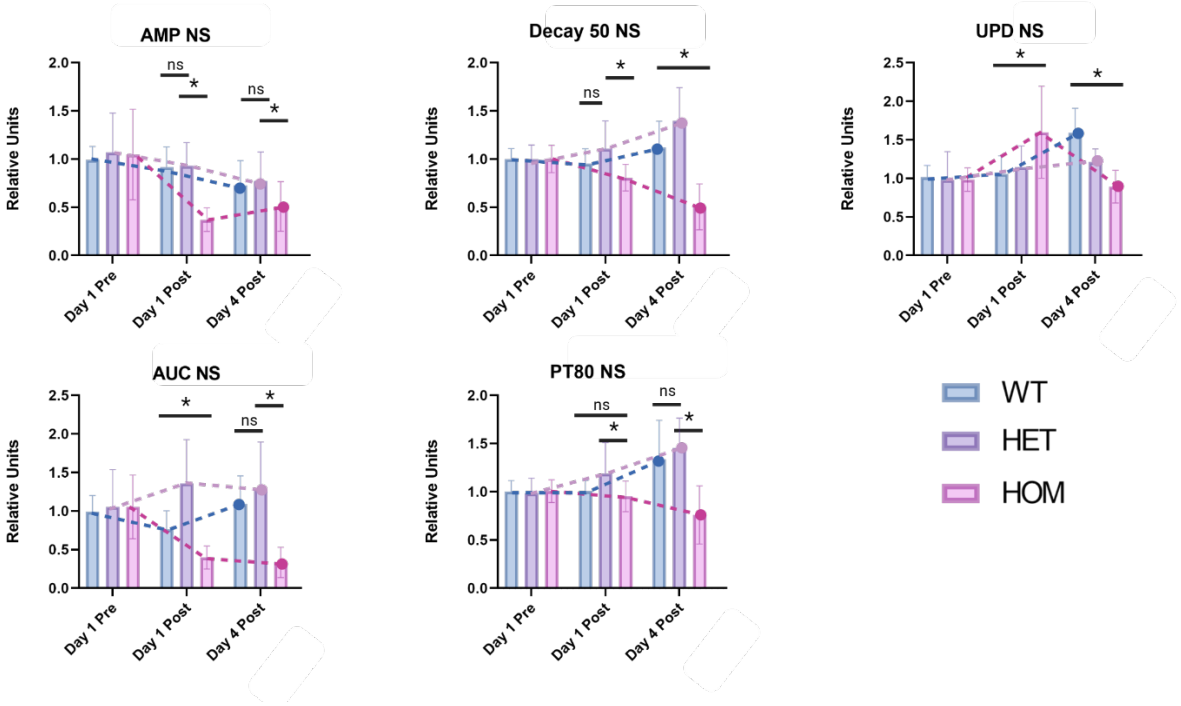

Figure 4.10: Compiled normalized results of waveform components in response to prolonged culturing between the non-stretched isotypes. A Student's t-test was used for finding statistical significance between groups. NS = "non-stretched". N = 20. P-values are reported as $p < 0.05$ (*) and $p > 0.05$ (ns). Graphs were made using BioRender (biorender.com).

Initially, variation among amplitude for the duration of culturing was evaluated on the PDMS substrate among the non-stretch (NS) group. The WT and HET groups displayed no significant variation, while the HOM group demonstrated a significantly lower amplitude, especially on the Day 1 and 4 post-stretch time points. Differences in Decay 50 times were significant between the HET and HOM groups at Day 1 post stretch. The remaining time points

also experienced significant differences with HOM generally having the lowest time out of the three. Similarly, uptick duration among isotypes was varied to a significant degree ###. Total calcium handling or area (AUC) was generally the lowest in the HOM isotype while the WT and HET groups remained consistent. Also worth noting is that most isotypes displayed similar peak handling time or PT80. Minus the relationship between HOM and HET groups, in which case HET hiPSC-CMs saw a generally higher increase in these times.

The stretched group was then investigated to determine the extent of how applied mechanical strain impacts calcium handling between the three isotypes. Maximum amplitude seemed to vary significantly among the groups, especially with the HET group finishing the experiment with an overall increase and the HOM group decreasing. The HOM group did not seem to recover over time, unlike the control group. However, the HOM group seemed to not have its Decay 50 time impacted by the induction of stretch. Both HET and WT groups appeared to have this value decrease as a response to the stretching, following a similar pattern to each other. Day 7 post stretching displayed the most variance between the isotypes. Uptick duration only experienced variance until Day 4 after stretching and onward. The WT and HOM had longer observed times as opposed to the HET group. As for total calcium flux occurring, WT closely mirrored the response of the HOM group, with the values remaining relatively constant throughout the duration of the experiment. Finally, peak amplitude times of the HOM group were significantly higher in response to stretching when compared to the other isotypes, and resulted in the slowest handling times. Both HET and WT followed a similar trend in response.

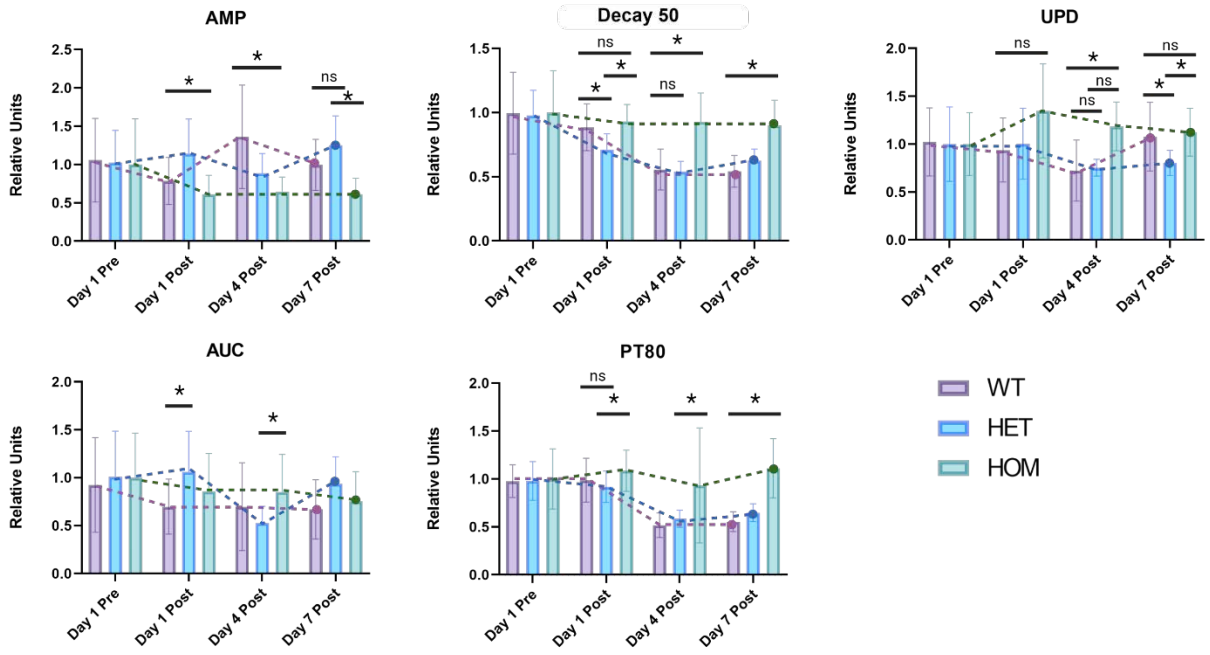

Figure 4.11: Compiled normalized results of waveform components in response to prolonged stretching between the isotypes. A Student's t-test was used for finding statistical significance between groups. N = 20. P-values are reported as p < 0.05 (*) and p > 0.05 (ns). Graphs were made using BioRender (biorender.com).

Table 4.1: Waveform characteristics are charted to summarize noteworthy changes to calcium cycling patterns after the induction of constant static stretching."*" denotes a significant difference when compared to the non-stretch group.

Waveform Characteristic	Acute Response to Stretching	Chronic Stretching Response
Amplitude	WT: Slight decrease. HET: No change. HOM: Decrease.	WT: Recovery, no net significant change.* HET: No significant change. HOM: No Recovery, net loss.
Decay 50%	WT: No change. HET: Decrease.* HOM: No change.	WT: Net reduction.* HET: Gradual reduction.* HOM: No net change.*
Uptick Duration	WT: No change. HET: No change. HOM: Increase.*	WT: Stagnated, no net change.* HET: No significant change.* HOM: Net increase.*
Area Under Curve	WT: Decreases. HET: No change.* HOM: No change.*	WT: No significant change. HET: Stagnated.* HOM: Decrease.
Peak Time (>=80%)	WT: No change. HET: No change.* HOM: No change.	WT: Net reduction.* HET: Net reduction.* HOM: No change.

4.4 Immunostaining

To demonstrate the ability to investigate sub-cellular remodeling, various batches of stretchers were fixated following the duration of the study using paraformaldehyde as described previously. Membranes were stained with fluorescently conjugated antibodies to reveal the structure and arrangement of sarcomeres within the hi PSC-CMs. To achieve this, antibodies were selected with specific binding to F-actin (green) and cTNT (red), vital components of the sarcomere thin filament and calcium-sensing complex respectively. Due to the current limitations of the platform, no direct comparisons will be made between isotypes due to the limited number and quality of the staining process. No sarcomere alignment was present on the membranes shown in Figure 4.12. However, sarcomere density did appear to be increased slightly in the stretched CMs, this being apparent by the visible quantity of F-actin present (Fig. 4.12). Although the differences were not statistically significant. Sarcomeres also appeared to cluster in regions among the stretched cells, indicating parallel sarcomere development and potential remodeling through redistribution of contractile power.

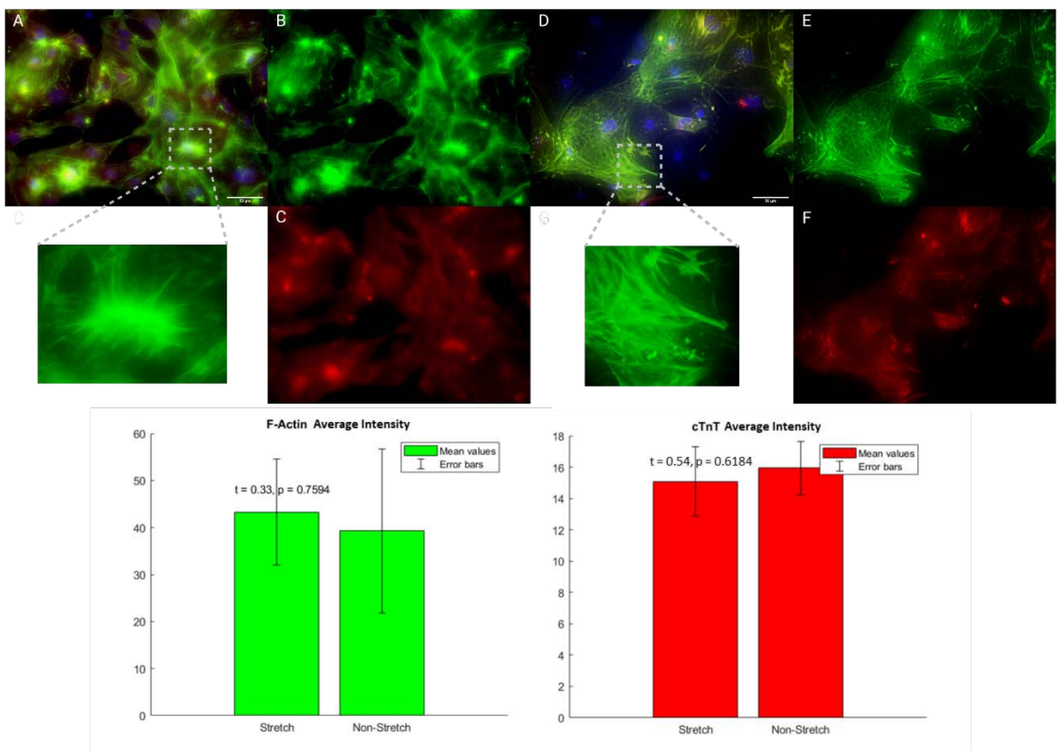

Figure 4.12: Fluorescent images of hiPSC-CMs taken at 40x magnification. Compiled stack image of hiPSC-CMs with a HET MYBPC3 mutation post-Day 7 of stretching (A) with stress fiber region zoomed to show detail. Standalone images of F-Actin (B) and cTNT (C) are also provided. Additionally, a compiled stack image of hiPSC-CMs with a HOM MYBPC3 mutation post Day 7 of culture without stretching (D). Sarcomeres zoomed in to show detail. Standalone images of F-Actin (E) and cTNT (F) are once again provided. Graphs of collective intensity from binding assay are shown below, N = 3.

4.5 Mathematic Simulation

The thickness of the membrane was estimated using information from Zhang et. al[29]. After stretching, the thin region of the membrane had a relatively uniform dispersion of stress and strain (Fig. 4.13). The 200µm thin substrate averaged $8.71*10^4$ N/m2 along its cross-sectional area. Therefore, we can represent this on a cellular level by converting units to conclude that for every 1 mm^2, a force of 0.0871 N was experienced on the cell's substrate via lateral stretching. As predicted, the strain was the highest towards the central region of the membrane forming an hourglass-like shape, where an average value of 0.099 (m/m) was recorded. While visible from the side profile view, there appeared to be a slight degree of downward bowing around the area where the rod attached to the slider would be. However, it did not seem to impact the planar surface of the cell seeding area.

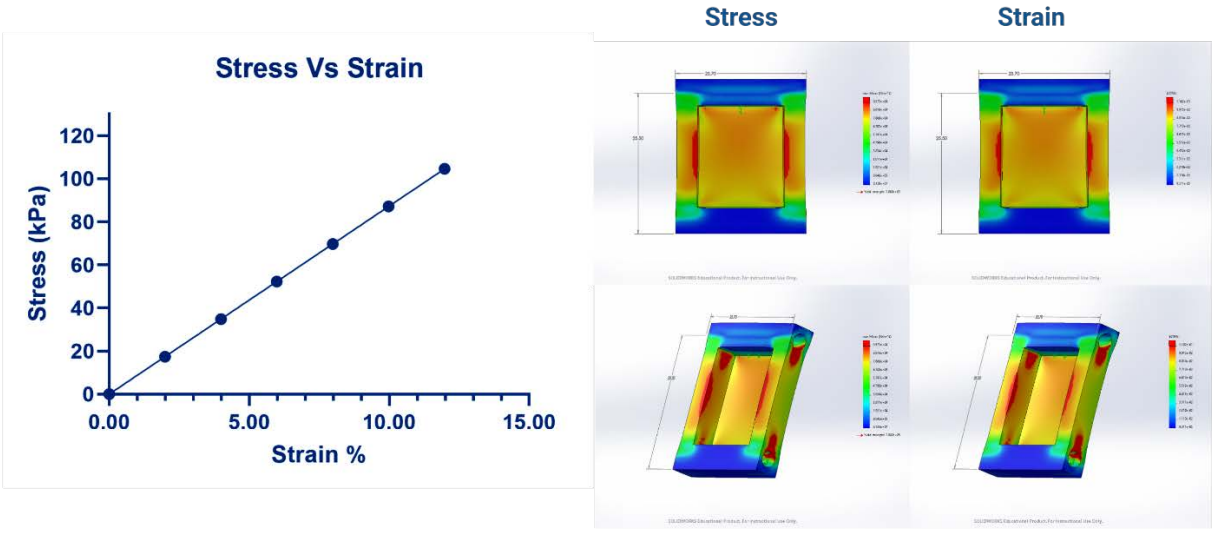

Figure 4.13: Graph depicting the linear relationship between derived stress and strain values during displacement caused by stretching. Images of the simulated membrane show a heat map of regionally experienced stress and strain.

Graphing the points revealed a linear relationship between stress (σ) and strain (ε). Therefore, we can model the system as a linear spring. Using the derived stress and strain values,

we can go on to calculate the average Young's Modulus of the membrane (E) by utilizing the equation:

$$E = (\sigma/\varepsilon)$$

In short, this formula is a form of Hooke's Law that utilizes the elastic modulus (σ/ε) we derived from the stress and strain values obtained respectively to determine the amount of force required to displace the material a certain quantity. This calculation yields a theoretical Youngs modulus of 872 kPa, regardless of stretching percentage. To confirm this value, a more precise measurement with a microcantilever or equivalent method is required.

CHAPTER 5

DISCUSSION AND FUTURE DIRECTIONS

5.1 Displacement Capabilities of the Stretcher

The stretcher platform appeared to be able to apply constant static stretching and produce strain percentages that can be experienced for short periods within the left ventricular myocardium of healthy patients[30]. While a nearly 10% loss is not ideal when looking to develop a model with precise control of parameters, an increased diameter of the facet where the rod is fitted on the slider as well as the thickening of the slider near this region will help to counter this. Changes in myocardium dimensions are often complicated and can reach percentage increases of 10% in hemodynamic load, as well as a near doubling in ventricle wall thickness[31,32]. While there remains a wide range of physiologic remodeling, more extreme cases are often coupled with a poor prognosis[33]. However, Yang et al. utilized this method of load induction to witness hypertrophic-like responses via sarcomere remodeling with 4-6% stretching[34]. Therefore, this places our utilized stretching percentage within the range of study for the HCM phenotype. The ability to model strain values encompassing HCM patients of varying severity demonstrates the potential to evaluate methods of pathogenesis and how they may differ from strain changes. While an advantage of this platform is its simplicity and reproducibility, the use of threaded machine screws offers a limited degree of control for displacement values. To increase the accuracy of the HCM conditions being modeled, the use of a linear actuator will be investigated. This also would seek to reduce the amount of physical handling required of the system through digitally controlled experiment parameters. Additionally, this would allow for both cyclic and static modes of stretching to take place. While cyclic stress has been utilized by a few groups such as Leychenko et al. to investigate the role of growth factor signaling[35], and Byun et al.

analyzing cell lysates post cyclic stretch exposure to characterize YAP localization[36], the need for an in-vitro model to incorporate the use of cyclic stretch to profile calcium dynamics remains unmet.

5.2 Seeding of Cells onto Stretcher

The disregard of the hiPSC-CMs towards the micropatterned features of the membrane demonstrates a serious limitation of the platform. Our lab has previously demonstrated the importance of alignment in the maturation of calcium dynamics and other cellular characteristics to better replicate in-vivo conditions[17]. With this understanding, a new patterning method must be investigated to capitalize on increasing hiPSC-CM maturity and the associated benefits. The usage of stencil-based patterning may hold the key to solving more than one problem of the current system. By directly differentiating hiPSCs on the PSMS membrane, disruptions to cellular mechanics and contamination can be reduced by avoiding extra passaging. The concept has already been proven in other applications and may benefit our current system to increase the consistency of data collection[37].

5.3 Calcium Image Analysis

Calcium image results implied a direct response from hiPSC-CMs by a prolonged static 12% strain. The WT group displayed signs of active remodeling calcium handling in response to the induction of stretch. This was characterized by the preservation of total calcium being cycled and recovery of waveform amplitude, while other characteristics such as Decay 50% and Peak Time experienced a reduction. However, AUC was lower by Day 7 after stretching when compared to its non-stretched counterpart, this is consistent with HCM patients exhibiting reduced ejection fractions during systolic contraction[38] and supports the notion that hypertrophic conditions are not met solely by genetic mutation of the sarcomere. This also may indicate that

increased hemodynamic pressure may stunt the mechanistic development of calcium handling in cardiomyocytes during development into adulthood.

Without the presence of stress, HET cells cultured on the PDMS membrane demonstrated higher Decay 50 times than their WT counterparts. These results agree with those of a recent publication by Pioner et al. as they found decay times decreased from carrying the MYBPC3 mutation in HET fashion[39]. The HET group interestingly exhibited many characteristic changes like that of the WT grouping in response to prolonged stretching, less so with its acute responses that appeared to be almost non-existent outside of a reduction in the decay time of the wave. However, stretching did seem to impact the maturity and overall shape of the waveform when compared to the non-stretched group. This may indicate that markers of CM maturation may be altered due to the induction of stress[40], much like what occurred in the WT group.

Unlike the other isotypes, hiPSC-CMs with a HOM mutation for MYBPC3 displayed the greatest hypertrophic response to static stretching. This was best characterized by an increase in decay times at Day 7 when compared to its non-stretched equivalent group, as slowed calcium handling in myocardial relaxation is a distinct marker of HCM. Additionally, both the acute chronic responses to stretching of the HOM cell line were much more apparent than that of the HET line and more like that of the WT, based on several significant differences from the non-stretched equivalent. Now comparing relative changes among stretched isotypes, we can see that the HOM group produced a much flatter curve than the others. This indicates a reduced sensitivity of the sarcomere to calcium, consistent with a dysfunctional calcium apparatus. Most notably, the induction of stretching appeared to amplify the shape of this waveform as indicated by increased decay duration times, increased peak width (PT80), and a similar curve area when compared to the non-stretched group. These findings demonstrate the ability of the stretcher

platform to investigate the varying routes of pathogenesis among the different isotypes.

5.4 Immunostaining

As mentioned previously, limited samples of fluorescently stained samples were available due to a combination of poor calcium viability of the hiPSC-CMs and the geometry of the stretcher itself. Many batches were lost due to dehydration or calcium handling disruptions. From what was obtained, no direct comparisons can be made due to the presence of differing variables. For example, the images displayed previously spotlight sarcomere structures of both HET and HOM groups that were stretched and not stretched, in respective order. The lack of cellular alignment was again confirmed by the F-actin stain. However, the stretched HOM hiPSC-CMs demonstrated an increased presence of stress fibers as visible from both the F-Actin and TNNT stains. These findings are consistent with the production of more focal adhesion sites, as confirmed by previous studies indicating increased expression of mechanotransduction-related proteins in response to hypertrophic conditions[41,42]. To investigate if this holds true with the other cell isotypes, the reproducibility of results is paramount. Achieving this will be done through dissection of the membranes post staining and mounting onto glass cover slides.

While components adjacent to integrin signaling are important, the inclusion of stains for the most central downstream effector of the Hippo pathway YAP/TAZ will best serve to further quantify increased mechanotransduction pathway expression and localization. Studies aimed at better characterizing the Hippo pathway have demonstrated the role of YAP/TAZ in mechanotransduction in relaying cytoskeletal tension to dictate cellular outputs to mechanical stimuli[43,44]. Nuclear localization of YAP through an increase in stiffness has also suggested heightened transcriptional activation and only further emphasizes its importance in mechanotransduction on dynamic substrate conditions. A further understanding of how

hypertrophy is mediated by mechanical stimuli and increasing cytoskeletal strain will help us to further craft our model into an accurate and efficient system for studying HCM *in-vitro*.

CHAPTER 6

CONCLUSION

In conclusion, this system has demonstrated the potential to apply a constant, static strain to healthy and mutated hiPSC-CMs for the MYBPC3 protein to model HCM in-vitro. The differences observed from not only the induction of stretching but also among isotypes, provide interesting findings and may offer key insights into the importance of genetic inheritance for HCM. Looking forward, both the enhancement of hiPSC-CM maturity and consistency of data collection are critical to developing an accurate and versatile disease modeling system. While the stiffness of the membrane is currently unable to be changed from stretching, the incorporation of a stiffness-changing hydrogel can add an extra dimension of hypertrophic-like conditions to the model. Additionally, the usage of RNA analysis in future studies can give better insight into transcriptional differences among different isotypes. This is especially important in the context of identifying mechanotransduction alterations and how they may play a role in the pathogenesis of hiPSC-CMs both carrying heterozygous and homozygous mutations for the MYCBPC3 protein.

REFERENCES

1. Wolf, C. M. & Cordula, M. W. Hypertrophic cardiomyopathy: genetics and clinical perspectives. *Cardiovasc Diagn Ther* **9**, (2019).

2. Shoucri, R. M. Active and passive stresses in the myocardium. *Am. J. Physiol. Heart Circ. Physiol.* **279**, (2000).

3. Ho, C. Y. *et al.* Myocardial Fibrosis as an Early Manifestation of Hypertrophic Cardiomyopathy. *N. Engl. J. Med.* **363**, 552–563 (2010).

4. Maron, B. J. *et al.* Prevalence of Hypertrophic Cardiomyopathy in a General Population of Young Adults. *Circulation* **92**, 785–789 (1995).

5. Semsarian, C., Ingles, J., Maron, M. S. & Maron, B. J. New Perspectives on the Prevalence of Hypertrophic Cardiomyopathy. *J. Am. Coll. Cardiol.* **65**, 1249–1254 (2015).

6. Shi, Y., Inoue, H., Wu, J. C. & Yamanaka, S. Induced pluripotent stem cell technology: a decade of progress. *Nat. Rev. Drug Discov. 2016 162* **16**, 115–130 (2016).

7. Richard, P. *et al.* Hypertrophic Cardiomyopathy. *Circulation* **107**, 2227–2232 (2003).

8. Wessels, M. W. *et al.* Compound heterozygous or homozygous truncating MYBPC3 mutations cause lethal cardiomyopathy with features of noncompaction and septal defects. *Eur. J. Hum. Genet.* **23**, 922–928 (2015).

9. Luther, P. K. *et al.* Direct visualization of myosin-binding protein C bridging myosin and actin filaments in intact muscle. *Proc. Natl. Acad. Sci. U. S. A.* **108**, 11423–11428 (2011).

10. Alamo, L. *et al.* Effects of myosin variants on interacting-heads motif explain distinct hypertrophic and dilated cardiomyopathy phenotypes. *Elife* **6**, (2017).

11. Barefield, D. *et al.* Haploinsufficiency of MYBPC3 Exacerbates the Development of Hypertrophic Cardiomyopathy in Heterozygous Mice. *J. Mol. Cell. Cardiol.* **79**, 234 (2015).

12. Seeger, T. *et al.* A premature termination codon mutation in MYBPC3 causes hypertrophic cardiomyopathy via chronic activation of nonsense-mediated decay. *Circulation* **139**, 799–811 (2019).

13. Van Dijk, S. J. *et al.* Cardiac myosin-binding protein C mutations and hypertrophic cardiomyopathy: haploinsufficiency, deranged phosphorylation, and cardiomyocyte dysfunction. *Circulation* **119**, 1473–1483 (2009).

14. Voorhees, A. P. & Han, H. C. Biomechanics of cardiac function. *Compr. Physiol.* **5**, 1623–1644 (2015).

15. Zhao, X. & Guan, J. L. Focal adhesion kinase and its signaling pathways in cell migration

and angiogenesis. *Adv. Drug Deliv. Rev.* **63**, 610–615 (2011).

16. Taylor, J. M., Rovin, J. D. & Parsons, J. T. A role for focal adhesion kinase in phenylephrine-induced hypertrophy of rat ventricular cardiomyocytes. *J. Biol. Chem.* **275**, 19250–19257 (2000).

17. Strimaityte, D. *et al.* Contractility and Calcium Transient Maturation in the Human iPSC-Derived Cardiac Microfibers. *ACS Appl. Mater. Interfaces* **14**, 35376–35388 (2022).

18. Corbin, E. A. *et al.* Tunable and Reversible Substrate Stiffness Reveals a Dynamic Mechanosensitivity of Cardiomyocytes. *ACS Appl. Mater. Interfaces* **11**, 20603–20614 (2019).

19. Martewicz, S. *et al.* Transcriptomic Characterization of a Human In Vitro Model of Arrhythmogenic Cardiomyopathy Under Topological and Mechanical Stimuli. *Ann. Biomed. Eng.* **47**, 852–865 (2019).

20. Becker, B. *et al.* Magnetic Adjustment of Afterload in Engineered Heart Tissues. *J. Vis. Exp.* **2020**, (2020).

21. Dong, S. J. *et al.* Left ventricular wall thickness and regional systolic function in patients with hypertrophic cardiomyopathy. A three-dimensional tagged magnetic resonance imaging study. *Circulation* **90**, 1200–1209 (1994).

22. Becker, R. C., Owens, A. P. & Sadayappan, S. Tissue-level inflammation and ventricular remodeling in hypertrophic cardiomyopathy. *J. Thromb. Thrombolysis* **49**, 177–183 (2020).

23. Van Dijk, S. J. *et al.* Contractile dysfunction irrespective of the mutant protein in human hypertrophic cardiomyopathy with normal systolic function. *Circ. Hear. Fail.* **5**, 36–46 (2012).

24. Bers, D. M. Cardiac excitation–contraction coupling. *Nature* **415**, 198–205 (2002).

25. Lehman, W., Craig, R. & Vibert, P. Ca2+-induced tropomyosin movement in Limulus thin filaments revealed by three-dimensional reconstruction. *Nat. 1994 3686466* **368**, 65–67 (1994).

26. Liao, J. *et al.* A novel Ca2+ indicator for long-term tracking of intracellular calcium flux. *Biotechniques* **70**, (2021).

27. Smith, N. A. *et al.* Fluorescent Ca2+ indicators directly inhibit the Na,K-ATPase and disrupt cellular functions. *Sci. Signal.* **11**, 2039 (2018).

28. Ma, Z. *et al.* Contractile deficits in engineered cardiac microtissues as a result of MYBPC3 deficiency and mechanical overload. *Nat. Biomed. Eng.* **2**, 955–967 (2018).

29. Zhang, W. Y., Ferguson, G. S. & Tatic-Lucic, S. Elastomer-supported cold welding for

room temperature wafer-level bonding. *Proc. IEEE Int. Conf. Micro Electro Mech. Syst.* 741–744 (2004) doi:10.1109/MEMS.2004.1290691.

30. Caracciolo, G. *et al.* Myocardial stretch in early systole is a key determinant of the synchrony of left ventricular mechanical activity in vivo. *Circ. J.* **77**, 2526–2534 (2013).

31. Strachinaru, M. *et al.* Myocardial Stretch Post-atrial Contraction in Healthy Volunteers and Hypertrophic Cardiomyopathy Patients. *Ultrasound Med. Biol.* **45**, 1987–1998 (2019).

32. Dong, S. J. *et al.* Left ventricular wall thickness and regional systolic function in patients with hypertrophic cardiomyopathy: A three-dimensional tagged magnetic resonance imaging study. *Circulation* **90**, 1200–1209 (1994).

33. Hiemstra, Y. L. *et al.* Global Longitudinal Strain and Left Atrial Volume Index Provide Incremental Prognostic Value in Patients with Hypertrophic Cardiomyopathy. *Circ. Cardiovasc. Imaging* **10**, (2017).

34. Yang, H. *et al.* Dynamic Myofibrillar Remodeling in Live Cardiomyocytes under Static Stretch. *Sci. Rep.* **6**, (2016).

35. Leychenko, A., Konorev, E., Jijiwa, M. & Matter, M. L. Stretch-Induced Hypertrophy Activates NFkB-Mediated VEGF Secretion in Adult Cardiomyocytes. *PLoS One* **6**, e29055 (2011).

36. Byun, J. *et al.* Yes-associated protein (YAP) mediates adaptive cardiac hypertrophy in response to pressure overload. *J. Biol. Chem.* **294**, 3603–3617 (2019).

37. Wang, B., Tu, X., Wei, J., Wang, L. & Chen, Y. Substrate elasticity dependent colony formation and cardiac differentiation of human induced pluripotent stem cells. *Biofabrication* **11**, 015005 (2018).

38. Liu, C. P. *et al.* Diminished contractile response to increased heart rate in intact human left ventricular hypertrophy: Systolic versus diastolic determinants. *Circulation* **88**, 1893–1906 (1993).

39. Pioner, J. M. *et al.* Slower Calcium Handling Balances Faster Cross-Bridge Cycling in Human *MYBPC3* HCM. *Circ. Res.* **132**, 628–644 (2023).

40. Bedada, F. B., Wheelwright, M. & Metzger, J. M. Maturation status of sarcomere structure and function in human iPSC-derived cardiac myocytes. *Biochim. Biophys. Acta - Mol. Cell Res.* **1863**, 1829–1838 (2016).

41. Torsoni, A. S., Constancio, S. S., Nadruz, W., Hanks, S. K. & Franchini, K. G. Focal Adhesion Kinase Is Activated and Mediates the Early Hypertrophic Response to Stretch in Cardiac Myocytes. *Circ. Res.* **93**, 140–147 (2003).

42. Thievessen, I. *et al.* The focal adhesion protein β-parvin controls cardiomyocyte shape and sarcomere assembly in response to mechanical load. *Curr. Biol.* **32**, 3033-3047.e9 (2022).

43. Wada, K. I., Itoga, K., Okano, T., Yonemura, S. & Sasaki, H. Hippo pathway regulation by cell morphology and stress fibers. *Development* **138**, 3907–3914 (2011).

44. Dupont, S. *et al*. Role of YAP/TAZ in mechanotransduction. *Nat. 2011 4747350* **474**, 179–183 (2011).